Computational modeling of the effects of EEG volume conduction on functional connectivity metrics. Application to Alzheimer's disease continuum

Saúl J. Ruiz-Gómez[1], Roberto Hornero[1,2], Jesús Poza[1,2], Aarón Maturana-Candelas[1], Nádia Pinto [3,4,5], Carlos Gómez[1]

[1] Biomedical Engineering Group, University of Valladolid, Valladolid, Spain
[2] IMUVA, Mathematics Research Institute, University of Valladolid, Valladolid, Spain
[3] IPATIMUP, Instituto de Patologia e Imunologia Molecular da Universidade do Porto, Porto, Portugal
[4] Instituto de Investigação e Inovação em Saúde, Porto, Portugal
[5] CMUP, Center of Mathematics of the University of Porto, Porto, Portugal.

E-mail: saul.ruiz@gib.tel.uva.es

Abstract. *Objective.* The aim of this study was to evaluate the effect of electroencephalographic (EEG) volume conduction in different measures of functional connectivity and to characterize the EEG coupling alterations at the different stages of dementia due to Alzheimer's disease (AD). *Approach.* Magnitude Squared Coherence ($MSCOH$), imaginary part of Coherence ($iCOH$), lagged Coherence ($lagCOH$), Amplitude Envelope Correlation (AEC), Synchronization Likelihood (SL), Phase Lag Index (PLI), Phase Locking Value (PLV), and corrected imaginary PLV ($ciPLV$) were applied to: (i) synthetic signals generated with a Kuramoto-based model of several coupled oscillators; and (ii) a resting-state EEG database of real recordings from 51 cognitively healthy controls, 51 mild cognitive impairment (MCI) subjects, 51 mild AD (AD_{mil}) patients, 50 moderate AD (AD_{mod}) patients, and 50 severe AD (AD_{sev}) patients. *Main results.* Our results using synthetic signals showed that PLI was the least affected parameter by spurious influences in a simulated volume conduction environment. Results using real EEG recordings showed that spontaneous activity of MCI patients is characterized by a significant coupling increase in the θ band. As dementia progresses, this increase in the θ band became more pronounced, and a significant widespread decrease in α band appeared at the last stage of dementia. *Significance.* Our results revealed that the estimation of functional EEG connectivity using PLI could reduce the bias introduced by the spurious influence of volume conduction, and it could increase the insight into the underlying brain dynamics at different stages of the AD continuum.

Keywords: Alzheimer's disease, mild cognitive impairment, electroencephalography (EEG), synthetic signals, volume conduction, neural coupling.

Submitted to: *J. Neural Eng.*

1. Introduction

The human brain contains billions of interconnected neurons forming a complex network of innumerable connections [1]. These networks are continuously changing and adapting themselves due to external and internal stimuli throughout the entire life span [2]. Specifically, the combination of different factors, such as synaptic pruning, the neuronal apoptosis, and the loss of cortico-cortical connections, is responsible for physiological brain aging [2]. However, some physiopathological processes can alter normal brain aging and cause dementia.

Dementia due to Alzheimer's disease (AD) is the most common cause of dementia, with an estimated 60–80% of cases [3]. Depending on the affected brain regions and the symptoms, different stages can be distinguished during the course of AD continuum. The initial symptoms of AD are usually preceded by a stage known as mild cognitive impairment due to AD (MCI). MCI subjects exhibit a memory impairment beyond what would be expected for their age, but do not fully accomplish the criteria for dementia diagnosis [4]. Therefore, MCI can be considered a prodromal stage of AD, since previous research has shown that the conversion rate to AD is approximately 15% per year [5], whereas healthy controls develop dementia at a rate of only 1–2% per year [3]. Then, in the earliest AD stage, known as mild AD (AD_{mil}), patients may function independently but they show symptoms as reading problems and clear deficits on clinical examination. In the next stage, moderate AD (AD_{mod}), patients require a greater level of care because they show increasingly poor judgment and deepening confusion. Finally, severe AD (AD_{sev}) is the last stage of this disease, in which patients loose the ability to respond to their environment and, eventually, to control movement.

During the last decades, several neuroimaging techniques have been used to detect brain changes associated with neurodegeneration and cognitive decline [6]. Methods like functional magnetic resonance imaging (fMRI) and positron emission tomography (PET) have been used to investigate functional and metabolic brain changes in AD and MCI [7, 8]. However, fMRI and PET do not offer enough temporal resolution to study real-time brain dynamics. In order to study the dynamical processes involved in complex brain systems, techniques with high temporal resolution, such as electroencephalography (EEG) and magnetoencephalography (MEG), are required [9]. Specifically, EEG is widely used in clinical settings to take advantage of its low cost and portability compared to MEG. Moreover, EEG has already shown its usefulness to characterize brain dynamics in AD and MCI [10, 11, 12, 13].

EEG measures the electrical activity generated by synchronized cortical neuronal pools with electrodes placed at the scalp [14]. However, these signals suffer from attenuation, expansion and noise contamination when traveling across different surfaces in the head. These effects cause that there is no unique solution when estimating the active neuronal sources in the brain from the time series recorded on the scalp [10]. This is known as 'volume conduction' problem and can provoke spurious correlations between time series recorded by nearby electrodes, because they are very likely to pick up electrical activity from the same brain sources, even if their are independent [10, 15]. In order to achieve a correct interpretation of the results, it is important to employ coupling metrics that do not yield significant connectivity estimations between independent sources [16]. Consequently, these connectivity estimations are indicators of real brain interactions, minimizing the effect of volume conduction distortion [17].

In order to simulate the neuronal current propagation from the source regions within the brain to the EEG electrodes, several electrical models have been proposed: from simple n-sphere models (in which each concentric spherical region represents different brain layers) to more accurate models based on information from other neuroimaging techniques [18]. To simulate the source activity, also different procedures have been used, such as dipole generators, potential meshes, and oscillators [10, 19, 18]. The most extended electrical model in EEG source analysis is the boundary element method (BEM) [20]. The BEM quasi-analytic solution can be obtained within n-shell geometry using spherical harmonics expansions (SHE) of the electric lead fields [21]. On the other hand, finite element based (FEM) approaches use real-head models assuming realistic information of where the different tissues (e.g. skin, skull, cerebrospinal fluid (CSF), gray and white matter) are inside the head [22, 23]. However, these methods do not allow the characterization of the influence of volume conduction in coupling estimators, since the simulation of ideal

scenarios without volume conduction is not feasible [10, 19]. A first approach to evaluate the influence of EEG volume conduction in different connectivity metrics was performed by *Stam et al.* [10], and another recent study replicated this one with the same limitations [19]. In both studies, brain source activity was simulated using the well-known Kuramoto model [24], a set of globally coupled limit-cycle oscillators centered at a single frequency of 10 Hz. This value was selected as it is the predominant frequency in resting-state eyes-closed EEG activity [10]. To model volume conduction, they proposed three different scenarios of increasing common sources by allowing more than a single oscillator to contribute to each simulated EEG channel [10]. They conclude that this approach allowed them to test the behavior of various measures under exaggerated effects of volume conduction, but in a quite simple way because modeling realistic sources in a volume conductor is beyond the scope of their study [10]. Starting from this point, we wanted to go a step further and simulate the brain activity with multiple oscillators centered at different frequencies within all the available EEG spectrum, as well as a more realistic model of the electrical propagation of the electric signals from sources to electrodes.

In the present study, we used the combination of a surface-based computational model of the human head obtained from anatomical cryosection images, and a model of coupled oscillators that simulate the electrical activity of brain sources. Then, two different scenarios were considered: the first one is a volume-conduction free case, while the other one is the real case with volume conduction. This model allows us to quantify how different functional connectivity metrics are affected by volume conduction. In this regard, eight measures, which have been developed to analyze neural connections, were evaluated: Magnitude Squared Coherence ($MSCOH$), imaginary part of Coherence ($iCOH$), lagged Coherence ($lagCOH$), Amplitude Envelope Correlation (AEC), Synchronization Likelihood (SL), Phase Lag Index (PLI), Phase Locking Value (PLV), and corrected imaginary PLV ($ciPLV$). Many previous EEG studies have focused on the application of different connectivity metrics, since local activation studies are no longer sufficient for a full characterization of AD brain dynamics [25]. Their results support the well-established hypothesis of AD as a 'disconnection syndrome' [2], but all these results may be biased due to volume conduction effects. Therefore, the aim of this study was to analyze which functional connectivity measures are able to detect real changes in synchronization without being affected by volume conduction and if they are able to characterize the brain alterations during AD continuum.

2. Materials

2.1. Subjects

In this study, resting-state EEG activity was recorded from a total of 253 subjects: 51 cognitively healthy control (HC) subjects, 51 MCI subjects, 51 AD_{mil} patients, 50 AD_{mod} patients, and 50 AD_{sev} patients. Firstly, information from the recordings of HC subjects, combined with the Kuramoto model and the real-head model, was used to create the synthetic data. Then, all recordings were used to study the neural interactions of the aforementioned stages during AD continuum.

Healthy controls had no pathological background, and underwent a cognitive assessment in order to discard any symptoms of neurological disorder. Patients with MCI and dementia due to AD were diagnosed following the criteria of the National Institute on Aging and Alzheimer's Association (NIA-AA) [26]. No significant differences between groups were found in age ($p > 0.05$, Kruskal-Wallis test). Socio-demographic and clinical data are provided in table 1.

This study was carried out in accordance with the recommendations of the Code of Ethics of the World Medical Association with written informed consent from all subjects. All subjects and caregivers gave written informed consent in accordance with the Declaration of Helsinki. The protocol was approved by the Ethics Committee of Porto University (Portugal).

2.2. EEG recordings

For each subject, five minutes of resting-state EEG activity were recorded using a 19-channel system at the electrodes Fp1, Fp2, Fz, F3, F4, F7, F8, Cz, C3, C4, T3, T4, T5, T6, Pz, P3, P4, O1, and O2 following the International System 10-20. Signals were recorded at a sampling frequency of 500 Hz using the Nihon Kohden Neurofax JE-921A system with common average reference (CAR).

Subjects were asked to remain awake with closed eyes during EEG acquisition. For each recording, the same pre-processing procedure was applied [13]. It consists of the following steps: (i) digital filtering using a Hamming window bandpass FIR filter in the band of interest (1–70 Hz) and a notch filter to remove the power line frequency interference (50 Hz); (ii) independent component analysis (ICA) to minimize the presence of oculographic, cardiographic, and myographic artifacts; and (iii) selection of 5-s artifact-free epochs by visual inspection.

Table 1. Socio-demographic and clinical data.

	HC	**MCI**	**AD$_{mil}$**	**AD$_{mod}$**	**AD$_{sev}$**
Number of subjects	51	51	51	50	50
Age (years) (mean±SD[a])	80.14±7.09	85.53±7.25	80.69±7.05	81.30±8.04	79.98±7.82
Gender (Male:Female)	26:25	15:36	21:30	7:43	7:43
MMSE[b] (mean±SD[a])	28.82±1.13	23.33±2.84	22.49±2.27	13.60±2.76	2.42±3.70

[a] SD: standard deviation; [b]MMSE, Mini Mental State Examination score; HC: cognitively healthy control subjects; MCI: Mild Cognitive Impairment patients; AD$_{mil}$: mild Alzheimer's disease patients; AD$_{mod}$: moderate Alzheimer's disease patients; AD$_{sev}$: severe Alzheimer's disease patients.

3. Methods

Our methodology is divided into the following steps:

(i) Firstly, the modeling of synthetic signals from the 19 simulated EEG channels is performed. We used a surface-based model built from information of the Visible Human Project® (VHP) dataset [27] (see Section 3.1). The electrical activity of brain sources was simulated using 200 oscillators forming a the Kuramoto model, where each oscillator represents the electrical activity generated by synchronized neuronal pools (see Section 3.2). The amplitude of the oscillators was determined based on the spectral content of HC subjects' EEG activity (see Section 3.3). Then, two different scenarios were simulated: the first one is a volume-conduction free case, while the second one is a simulated case with volume conduction (see Section 3.3).

(ii) Secondly, the selected eight connectivity metrics ($MSCOH$, $iCOH$, $lagCOH$, AEC, SL, PLI, PLV, and $ciPLV$) were computed for these two scenarios in order to quantitatively determine which of the analyzed connectivity metrics are able to detect real changes in synchronization without being affected by volume conduction. We used the Two-sample Kolmogorov-Smirnov test for this purpose (see Section 3.5).

(iii) Finally, for the chosen metrics in the previous step, coupling patterns were obtained for the five groups of our database. Then, statistical differences were evaluated between groups comparing healthy controls with each stage of dementia (MCI, AD$_{mil}$, AD$_{mod}$, and AD$_{sev}$).

3.1. Real-head model

In order to analyze the effect of volume conduction on the different functional connectivity metrics, we simulated synthetic signals using artificial sources inside the brain surface of a real-head model. Surface-based models describe each individual tissue as a triangular surface mesh. In this study, the surface-based computational model of the human head was constructed from the open-source Visible Human Project® (VHP) dataset [27]. The VHP dataset contains a large amount of magnetic resonance images, computed tomographies, and anatomical cryosection images from both males and females.

In our particular case, we used a previously created model described at [28]. This model is also available online at https://www.wiley.com/legacy/wileychi/makarov/matlab.html and has already been used in different studies to provide insight into the propagation of electromagnetic fields through the human head and transcranial direct current stimulation [29, 30].

This model used anatomical cryosection images from a patient in the construction of the model. These images have a resolution of 2048 x 1216 pixels, which corresponds with a spatial resolution of 0.33 mm. Then, the main structures of the head were identified and hand-segmented using ITK-Snap [31]. Specifically, the brain, the CSF, the skull, and the skin were identified. The results of this segmentation were very fine meshes with a large number of nodes for each tissue. Then, in order to reduce the computational cost of the simulations, the number of nodes was reduced, eliminating defects and discrepancies.

In this study, 19 simulated EEG electrodes were placed according to the International System 10-20. Thus, the final result of the real-head model is shown in figure 1. The electrical activity produced by synchronized neuronal pools generates electromagnetic waves (in our simulations, the electrical activity of each brain source is simulated with a coupled oscillator of the Kuramoto model). As the electromagnetic waves propagate from sources to electrodes, their amplitudes experience some attenuation. This attenuation defines the rate of amplitude loss of an electromagnetic wave defined by the parameter α (electrical attenuation). For each of the aforementioned modeled tissues, α was assigned according to: $\alpha_{brain} = 0.002726$, $\alpha_{CSF} = 0.016624$, $\alpha_{skull} = 0.001665$, and $\alpha_{skin} = 0.000165$. The procedure to compute α from relative permittivity and electrical conductivity values for

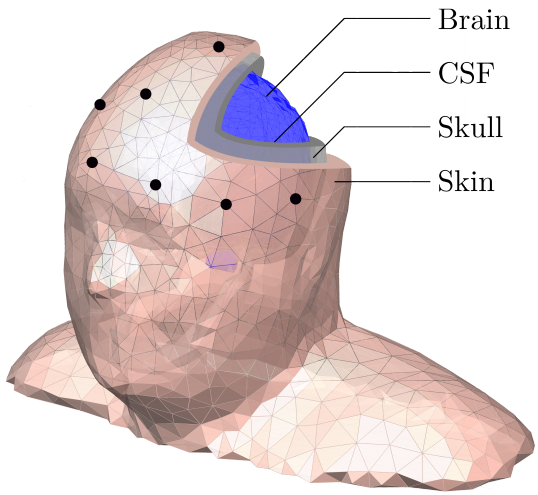

Figure 1. Real-head model from the VHP dataset [27].

each tissue (taken from Hasgal database, available at http://www.www.itis.ethz.ch/database) is detailed in the Table A of the Supplementary Material.

Once the model was created, the electrical activity of brain sources was simulated using a set of coupled oscillators forming a Kuramoto model.

3.2. Kuramoto model

The original model proposed by Kuramoto described the phase dynamics of N equally weighted and purely sinusoidal coupled oscillators. The phase dynamics of each oscillator is described by the following differential equation [24]:

$$\frac{d\theta_i}{dt} = \omega_i + \frac{K}{N}\sum_{j=1}^{N}\sin(\omega_j - \omega_i), \tag{1}$$

where θ_i represents the phase of the ith oscillator, whose natural frequency is ω_i, and K is the global coupling strength between all oscillators. This equation reflects that the phase evolution of each oscillator is determined by its natural frequency, ω_i, and the average influence of all other oscillators.

The natural frequencies ω_i are distributed according to some unimodal and symmetric probability distribution $g(\omega)$. Thus, the distribution should fulfill that $g(\omega) = g(-\omega)$ for all ω. Typically, Lorentzian distributions centered around ω_0 and with width γ are used to determine these natural frequencies [32]:

$$g(\omega) = \frac{\gamma}{\pi[\gamma^2 + (\omega - \omega_0)^2]}. \tag{2}$$

The global level of synchronization between the N oscillators that compose the system over time, $r(t)$, is defined as:

$$r(t) = \frac{1}{N}\sum_{j=1}^{N} e^{j\theta_i(t)}. \tag{3}$$

If the model is integrated numerically varying the global coupling K, two different scenarios appear. On one hand, for simulations with K less than a certain threshold K_{crit}, $r(t)$ evolves towards zero. This means that the oscillators act as if they were unsynchronized. On the other hand, when K exceeds K_{crit}, $r(t)$ grows exponentially, reflecting the emergence of a single cluster of synchronized oscillators [32]. As the natural frequencies are taken from a Lorentzian distribution, this critical value K_{crit} is only determined by the distribution width and is given by $K_{crit} = 2\gamma$ [10].

For each oscillator, equation (1) was numerically integrated using the Runge-Kutta method of order 4 [10]. Then, the state of the i-th oscillator, which was obtained from ω_0, at time t is given by:

$$O_{i,\omega_0}(t) = A_{\omega_0}\sin\theta_i(t), \tag{4}$$

where A_{ω_0} was a constant amplitude for all the oscillators obtained with the same ω_0, but frequency-dependent. The resulting time series represent the electrical activity of the brain sources.

3.3. Model simulations

Many parameters of the previously described Kuramoto model should be set for the simulation of the synthetic EEG signals that represent the electrical activity of the brain sources. Firstly, we divided the available spectrum of the real EEG signals from HC subjects (between 1 and 70 Hz) into spectral bands of 1 Hz wide. Then, we took the central frequencies ω_0 of each oscillator by evaluating the range $f_0 \in [1.5, 69.5]$ Hz (step=1 Hz), as $\omega_0 = 2\pi f$, as described in our previous work [33]. For each frequency band, a total number of $N = 200$ oscillators randomly placed inside the brain mesh were simulated, each one representing an active cerebral source. In order to extract analytical results, an infinite number of oscillators is needed, but it has been demonstrated that a limited number of them can be used to explain empirical results [34]. Also, this number of brain sources was determined as a trade-off that reduced computational costs and allowed every synthetic electrode to have a closest brain source. Specific oscillation frequencies were determined by a Lorentzian distribution of central frequency ω_0 and width $\gamma = 1$ [10, 19, 33].

The state of each oscillator was obtained by numerical integration with a time step of 2 ms (corresponding to a sample frequency of 500 Hz, according to the sample frequency of the real EEG recordings). With the aim of simulating the state of the oscillator $O_{i,\omega_0}(t)$, values of A_{ω_0} were determined

as the squared root of the relative power in each 1-Hz frequency band centered at ω_0, only taking into account real EEG recordings.

Then, we simulated two different scenarios:

(i) Firstly, an ideal volume-conduction free case in which each source is only registered by the closest EEG electrode. Thus, the voltage $V_j(t)$ of the jth simulated EEG channel at a time t was related to the state $O_{i,\omega_0}(t)$ of the ith oscillator (centered at ω_0) at a time t as:

$$V_j(t) = \sum_{\omega_0} \sum_{i} \sum_{\alpha} O_{i,\omega_0}(t) \cdot \mathrm{e}^{-\alpha \cdot d_{i,J}(\alpha)}, \tag{5}$$

with $d_{i,J} = \min(d_{i,j})$ for all j. α represents the electrical attenuation of each modeled tissues of the head, $d_{i,j}$ represents the total distance (in meters) between the simulated brain source i and the simulated EEG electrode j, and $d_{i,J}(\alpha)$ represents the distance (in meters) between the simulated brain source i and the simulated EEG electrode j in the modeled tissue with electrical attenuation α.

(ii) The second scenario represents the real-case with volume conduction, where each source activity is registered by all simulated EEG electrodes. Therefore, the voltage $V_j(t)$ can be defined as:

$$V_j(t) = \sum_{\omega_0} \sum_{i} \sum_{\alpha} O_{i,\omega_0}(t) \cdot \mathrm{e}^{-\alpha \cdot d_{i,j}(\alpha)}, \tag{6}$$

For each value of global coupling K, 300 trials were simulated, resulting 300 time series of 19 simulated channels and 2500 samples. It is noteworthy that in all trials, the initial 5000 samples were discarded to eliminate transitory states of the oscillators.

3.4. Functional connectivity metrics

Functional connectivity between each pair of electrodes was estimated using eight different functional coupling metrics, complementary from the point of view of the inference process: *MSCOH*, *iCOH*, *lagCOH*, *AEC*, *SL*, *PLI*, *PLV*, and *ciPLV*.

MSCOH is a well-known method that combines sensitivity to both amplitude and phase synchrony based on the normalized cross-spectral density. Given two time series X and Y two time series (from two different EEG channels), it is defined as [35]:

$$MSCOH_{X,Y} = |COH_{X,Y}|^2 = \frac{|S_{XY}|^2}{P_X P_Y}, \tag{7}$$

where S_{XY} is the cross-spectrum of X and Y, and P_X and P_Y are the power spectral density of X and Y respectively.

iCOH is the result of the projection of $COH_{X,Y}$ into the imaginary axis. Its main advantage is that it rules out instantaneous interactions, which may be due to volume conduction [36]. Its mathematical formulation reads:

$$iCOH_{X,Y} = \Im\{COH_{X,Y}\}, \tag{8}$$

where $\Im\{\cdot\}$ represents the imaginary part.

lagCOH was proposed by Pascual-Marqui *et al.* [37] to estimate connectivity between different brain regions removing the instantaneous contribution, which could be mainly due to volume conduction. It is defined as [37]:

$$lagCOH_{X,Y} = \frac{[\Im\{S_{X,Y}\}]^2}{S_X S_Y - \Re\{S_{XY}\}^2}, \tag{9}$$

where $\Re\{\cdot\}$ represents the real part.

AEC estimates the correlation of two signals based on their amplitudes. Firstly, time series are orthogonalized for each trial separately [38]. Then, their power envelopes are obtained using the Hilbert transform. Finally, coupling is calculated as the Pearson correlation between the *log*-transformed power envelopes [39].

SL represents the likelihood that if a system is in the same state at two different times, another system will also be in the same state at these two times. The detailed mathematical procedure to compute *SL* proposed by Stam *et al.* can be found in [40].

PLI was also proposed by Stam *et al.* [10] to overcome *SL* limitations and quantifies the asymmetry of the phase difference distributions of two signals. It is non sensitive to shared signals at zero phase lag, and the stronger this nonzero phase locking is, the larger the *PLI* will be. Mathematically, it is defined as [10]:

$$PLI_{X,Y} = |\langle sign \sin(\Delta\phi_{X,Y})\rangle|, \tag{10}$$

where $\langle\cdot\rangle$ indicates the expectation operator and $\Delta\phi_{X,Y}$ is the phase difference or relative phase between signals X and Y.

PLV is a time-dependent connectivity measure that looks for latencies at which the phase difference between the signals varies little across trials [41]. For resting-state data, it is defined as [42]:

$$PLV_{X,Y}(t) = \frac{1}{T}|\sum_{t=1}^{T} e^{-i(\phi_X(t)-\phi_Y(t))}|, \tag{11}$$

where T is the data length and ϕ is the instantaneous phase of the signals X and Y at time t.

ciPLV was proposed by Bruña *et al.* [43] to remove the contribution of the zero phase differences of *PLV*. Thus, this measure is insensitive to zero-lag effects and it is corrected in a similar way to *lagCOH*. Mathematically, it is defined as [43]:

$$ciPLV_{X,Y}(t) = \frac{\frac{1}{T}\Im\{e^{-i(\phi_X(t)-\phi_Y(t))}\}}{\sqrt{1-(\frac{1}{T}\Re\{e^{-i(\phi_X(t)-\phi_Y(t))}\})^2}} \tag{12}$$

3.5. Statistical and classification analyses

Firstly, in order to evaluate the influence of volume conduction with synthetic data, Two-sample Kolmogorov-Smirnov test (ks statistic) was used. The lower the values of ks, the lesser the differences between both curves. Specifically, the red curve corresponds to volume-conduction free case and the blue one to the real-case with volume conduction. Therefore, the more similar the curves of volume-conduction free scenario and the real case scenario with volume conduction are, the metric has a better behavior detecting real changes in synchronization without being affected by volume conduction.

Then, an exploratory analysis was carried out to assess the distribution of the coupling values with the real EEG recordings. As our results did not meet the parametric test assumptions of normality (Shapiro-Wilk test) and homoscedasticity (Levene's test), statistical differences between healthy control subjects and the rest of the groups were evaluated with the Mann-Whitney U-test. In order to deal with multiple simultaneous comparisons, a false discovery rate (FDR) controlling procedure was applied [44].

Finally, a classification approach using a leave-one-out cross validation procedure was performed to evaluate the clinical value of our metrics. As the characterization of the EEG may lead to the extraction of several redundant features, a feature selection stage based on stepwise multilinear regression with a conditional forward selection approach was included to select an optimal set of features. Afterwards, a linear discriminant analysis (LDA) was used to classify the subjects [45].

4. Results

4.1. Model simulations

Before any further analyses, we performed a qualitative analysis of the generated synthetic signals comparing them with the real EEG signals in the frequency domain by means of the normalized power spectral density (PSD_n), and in the time domain by visual inspection. Figure 2 displays the grand-averaged PSD_n across trials and all channels for a real HC subject (figure 2.a), and a the grand-averaged PSD_n across trials and all simulated channels for a synthetic signal generated with the Kuramoto model (figure 2.b). Grand averaged PSD_n from real EEG signals and from synthetic signals are very similar. Similarity between real and synthetic signals is also supported by two randomly selected 5-s EEG epochs from all channels, as figure 2 also shows.

Then, in order to determine the coupling metric that is less affected by volume conduction, all metrics were calculated from the time series generated with the Kuramoto model as a function of coupling strength K for the different scenarios. Connectivity results are summarized in figure 3, where the solid lines indicate the average coupling values over all pairs of the 19 simulated channels, and the shaded areas represent the standard deviation of the 300 simulated epochs.

Firstly, the results for $MSCOH$, $iCOH$, and $lagCOH$ are shown in figures 3.a, 3.b, and 3.c, respectively. In the scenario without volume conduction, $MSCOH$ stayed constant but higher than 0.2 for K lower than $K_{crit} = 2$ (when the expected value should be 0), and then increased for higher values of K, as expected from theory. When volume conduction was introduced in the second scenario, the resulting curve was shifted toward higher $MSCOH$ values showing that $MSCOH$ was very affected by spurious influences of common sources ($ks = 0.56$). Both $iCOH$ and $lagCOH$ stayed relatively constant around 0.04 and $lagCOH$ stayed constant for K lower than K_{crit}, and then increased for higher values of K in both scenarios. Furthermore, they also were slightly affected by volume conduction ($ks = 0.15$ and $ks = 0.16$, for $iCOH$ and $lagCOH$ respectively).

Secondly, figure 3.d shows that AEC stayed stable around 0.1 for $K < K_{crit}$ in both simulated scenarios. For $K > K_{crit}$, AEC started to increase slowly, never reaching values much higher than 0.2. When volume conduction was introduced, AEC became slightly lower for all values of K. Thus, AEC is slightly underestimating the true level of coupling. Quantitatively, the test statistic ks showed that AEC is not highly affected by volume conduction ($ks = 0.3$).

Thirdly, figures 3.e and 3.f show the SL and PLI results, respectively. In both scenarios, SL values remained very low for $K < K_{crit}$, and slightly increased from K_{crit} onwards. However, SL was the metric most affected by the spurious influences of common sources as the resulting curve was shifted toward higher SL values when volume conduction was introduced, as it showed the highest value of ks, 0.61). Figure 3.f shows the PLI results. In both scenarios, PLI values remained very low for $K < K_{crit}$, and increased from K_{crit} onwards. However, it can be noticed that PLI started to increase at $K = 1.5$, rather than at the theoretic value of $K_{crit} = 2$. When the influence of volume conduction is added, average PLI values were very similar for $K > K_{crit}$ compared with the volume conduction free scenario. Furthermore, PLI is slightly affected by the spurious influence of volume conduction as revealed by the test statistic ks ($ks = 0.12$).

Finally, the results for PLV and $ciPLV$ are shown in figures 3.g and 3.h, respectively. PLV stayed constant but around 0.15 for K lower than K_{crit} in

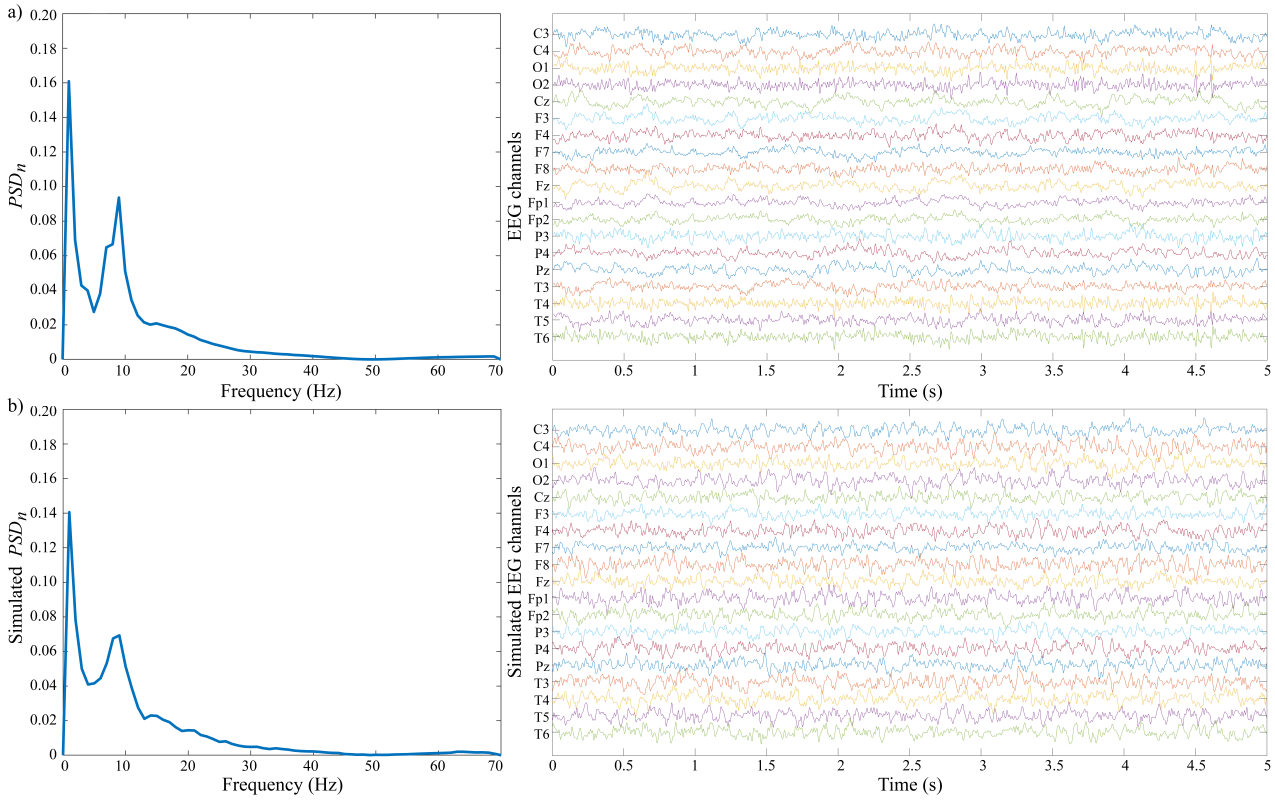

Figure 2. Normalized power spectral density (PSD_n) function grand-averaged over all trials and channels (left panels), and two random 5-s EEG epochs from all EEG channels (right panels): (a) HC subject, and (b) synthetic signal obtained with the Kuramoto model (simulated scenario with volume conduction).

the scenario without volume conduction, and then slightly increased for higher values of K. For the second scenario, higher PLV values were obtained when oscillators were not coupled. Thus, PLV was very affected by the spurious influences of common sources ($ks = 0.55$). However, $ciPLV$ was able to overcome this limitation minimizing the volume conduction distortion as very similar values for both scenarios were obtained ($ks = 0.13$), starting with values around 0.06 for $K < K_{crit}$, and increasing $ciPLV$ values as K increased.

To summarize, our model simulations showed that the eight analyzed metrics are sensitive to increases in the coupling strength for $K > K_{crit}$. For K values lower than K_{crit}, $iCOH$, $lagCOH$, AEC, PLI and $ciPLV$ showed low values of connectivity in both simulated scenarios. However, $MSCOH$ showed higher values compared with PLI (over 0.2 against 0.06) in the volume-conduction free scenario and higher values compared with PLI (around 0.35 against 0.06) under volume conduction conditions. For K higher than K_{crit}, all metrics responded to increases in the coupling strength. $MSCOH$, SL, and PLV overestimated connectivity and were very affected by spurious influences of volume conduction, while PLI, AEC, and $ciPLV$ were weakly influenced by the simulated volume conduction and underestimated the real coupling level. Quantitatively, the two-sample Kolmogorov-Smirnov test revealed that PLI was the metric least affected by the spurious influence of volume conduction ($ks = 0.12$), although none of the analyzed metrics are immune to it. For these reasons, the subsequent analysis with the real EEG recordings was performed using only PLI.

4.2. Real EEG recordings

For the metric chosen using synthetic data (PLI), coupling patterns were obtained for the five groups of our database. The characterization of the different AD stages was assessed comparing healthy elderly controls with each stage of dementia.

Since results are frequency-dependent, PLI was computed for the six classical EEG-frequency bands: delta (δ, 1-4 Hz), theta (θ, 4-8 Hz), alpha (α, 8-13 Hz), beta-1 (β_1, 13-19 Hz), beta-2 (β_2, 19-30 Hz), and gamma (γ, 30-70 Hz). Connectivity patterns obtained for each frequency band are presented in figure 4. Only statistically significant connections between groups (FDR-corrected p-values$<$0.05, Mann-

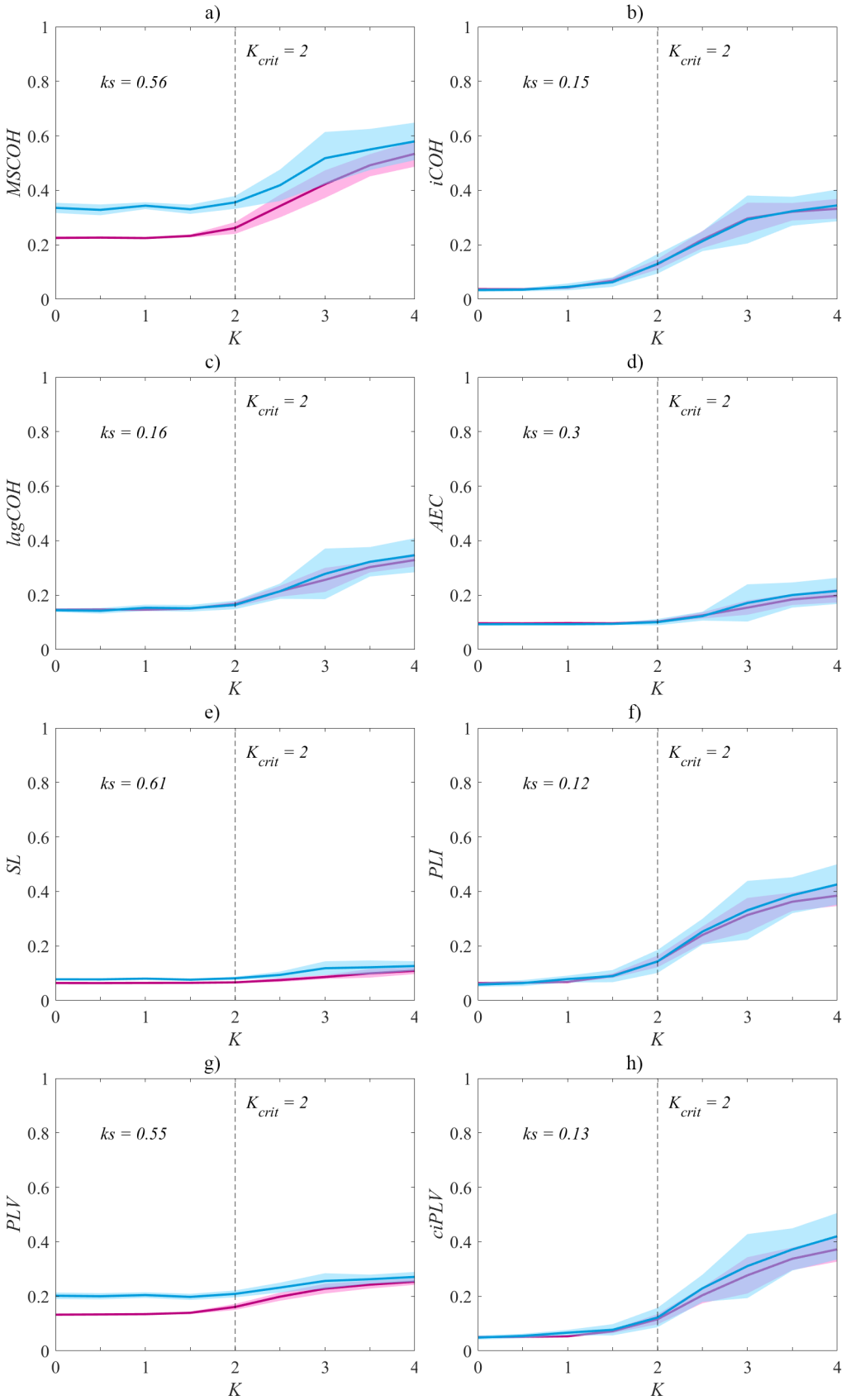

Figure 3. $MSCOH$, $iCOH$, $lagCOH$, AEC, SL, PLI, PLV, and $ciPLV$ values as a function of global coupling intensity (K) for the ideal volume-conduction free scenario (red) and the real-case with volume conduction scenario (blue). The solid lines indicate the average values and the shaded areas represent the standard deviation of the 300 simulated epochs. Two-sample Kolmogorov-Smirnov test values (ks statistic) are specified for each metric.

Whitney U-test) were displayed using the following color-code: red color tones indicated significant PLI increases in patients compared to controls, whereas blue color tones denoted significant decreases.

PLI results showed that EEG activity in MCI subjects is characterized by statistically significant connectivity increases in the θ band when compared to HC subjects, especially for long-distance interhemispheric connections. PLI increases in θ band were also found for the HC vs. AD_{mil} comparison after the FDR correction. Furthermore, some connections in the β_2 band showed significant connectivity decreases for AD_{mil} patients compared with HC subjects. The aforementioned trend of coupling increases in the θ frequency band as the disease progresses continued, reaching its maximum number of significant differences for the comparison between HC subjects and AD_{mod} patients. Additionally, our results revealed that AD_{sev} spontaneous EEG activity is characterized not only by widespread significant increases of PLI values in θ band, but also by an overall decrease of connectivity in α band. Finally, only a few connections showed statistically significant decreases in connectivity in β_2 band for AD_{sev} patients compared with HC subjects.

The combination of stepwise multilinear regression and LDA with a leave-one-out cross-validation procedure was used to assess the diagnostic value of our PLI results. The overall accuracy of the model in the five-class classification task was 41.50% (Cohen's kappa = 0.2688). Our model was also able to determine whether a subject is not healthy with an accuracy of 79.84% (Sensitivity = 86.63%; Positive Predictive Value = 84.85%). Furthermore, the model showed an accuracy of 77.47% when determining whether a subject suffer from AD (Sensitivity = 82.12%; Positive Predictive Value = 81.58%).

5. Discussion

In the present study, we evaluated the behavior of eight different functional connectivity metrics ($MSCOH$, $iCOH$, $lagCOH$, AEC, SL, PLI, PLV, and $ciPLV$) under the effect of volume conduction and their ability to characterize the brain alterations of the different stages during the AD progression.

5.1. Model simulations

In order to asses the effect of volume conduction and the changes in true synchronization, we used a surface-based computational model of the human head and a set of many coupled oscillators in a Kuramoto model. This combination allowed us to simulate the oscillatory nature of the EEG activity generated by brain sources and recorded at the scalp. The Kuramoto model behavior has been well-studied and it has been previously employed to simulate EEG activity [10, 19]. However, in these previous works they modeled volume conduction by allowing various oscillators contribute to each simulated EEG channel, because modeling realistic sources in a volume conductor was beyond the scope of the studies. As they concluded, this approximation was quite 'simplistically', but it allowed them for testing the behavior of different coupling metrics under extreme conditions [10, 19]. Starting from this point, we wanted to go a step further and simulate the brain activity with multiple oscillators centered at different frequencies within all the available EEG spectrum, as well as a more realistic model of the electrical propagation of the EEG signals from sources to electrodes.

Our connectivity results obtained with the synthetic signals showed that all analyzed metrics responded as expected from theory, reflecting the increases in coupling strength as continuously growing connectivity values for $K > K_{crit}$. Particularly, $iCOH$, PLI and $ciPLV$ were also able to quantify the synchronization between oscillators with lower K values and the bifurcation point at K_{crit} is less pronounced. Taking into account the lowest and highest coupling values obtained with the models for all these metrics, $MSCOH$, $iCOH$, PLI and $ciPLV$ had a relatively high dynamic range. Compared with them, the dynamic ranges of AEC and SL were much smaller, probably because our models were able to simulate a greater phase-based coupling instead of amplitude-based coupling. Qualitatively, when volume conduction was introduced in the simulations, our results showed that these effects were clearly smaller for $iCOH$, $lagCOH$, PLI and $ciPLV$. On the other hand, $MSCOH$, SL and PLV were strongly influenced by volume conduction, specially for low coupling strength values. After performing the quantitative analysis, it revealed that all eight metrics were not immune to volume conduction but these effects were clearly smaller for PLI. This result is closely related with the dynamic range of the metrics, since slight variations of $lagCOH$ and AEC due to volume conduction induced higher differences between both scenarios. However, similar variations of PLI produced less differences between scenarios, and it can be interpreted as PLI was less affected by volume conduction.

Comparing metrics from the point of view of the inference process, $iCOH$ and $lagCOH$ were proposed to remove instantaneous contributions, which could be mainly due to volume conduction [36, 37]. Our simulations showed that, as expected, both metrics were less affected by volume conduction compared to $MSCOH$. PLI was a new metric proposed by *Stam et al.* [10] to overcome limitations of SL, a previously described metric proposed also by them [40]. Our

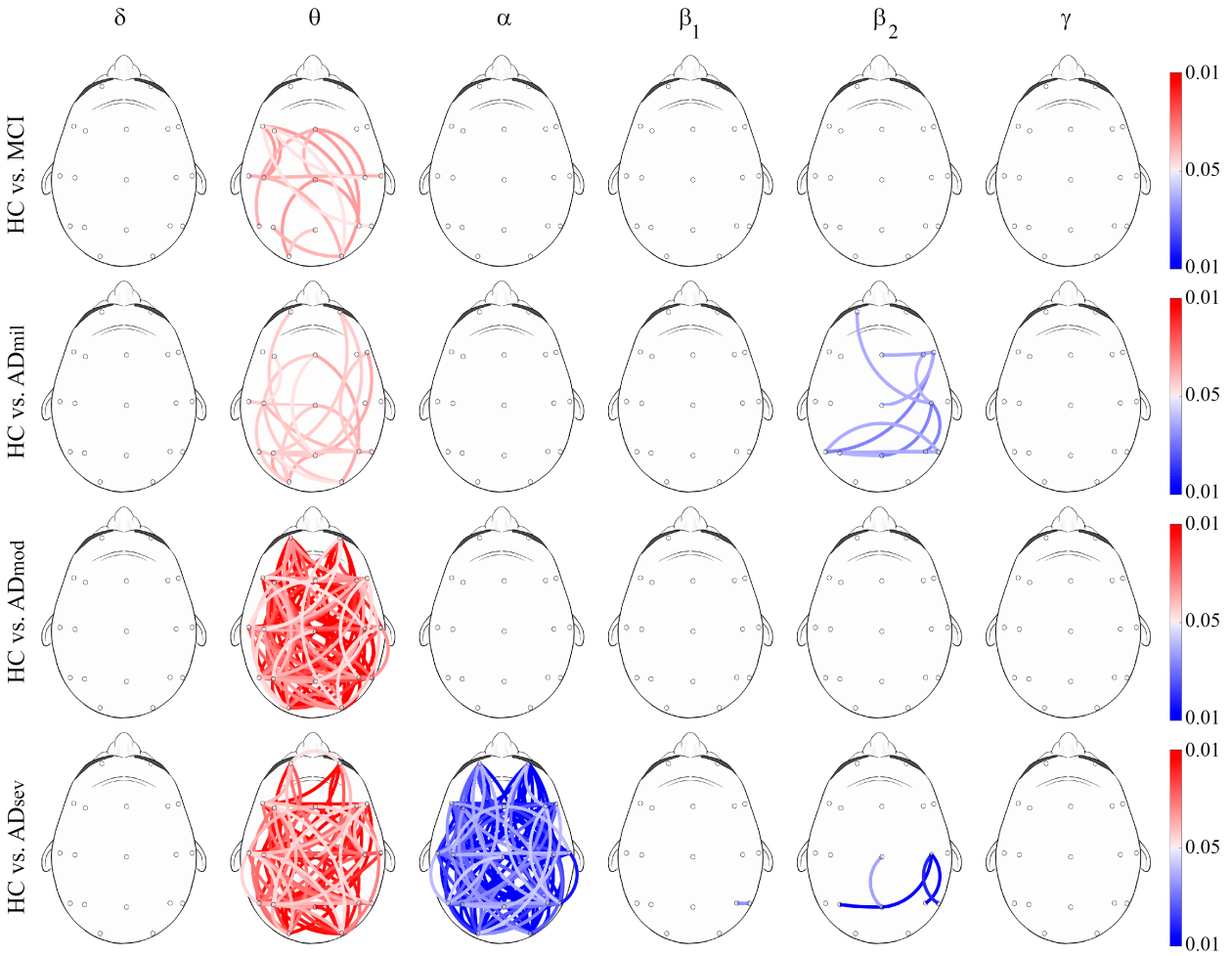

Figure 4. *PLI* results for each classical EEG-frequency band. Connections between electrodes were only displayed when statistically significant within group differences were obtained (Mann-Whitney U-test, FDR-corrected p-values < 0.05). Red color tones indicate statistically significant connectivity increases in patients compared to controls, whereas blue color tones denote significant decreases.

results also showed that PLI was able to minimize the effect of volume conduction distortion compared to SL. Following a similar way to remove the contribution of zero phase differences compared to $lagCOH$, $ciPLV$ was proposed as a PLV modification to overcome its limitations [43]. Our results showed that $ciPLV$ stayed less affected by volume conduction distortion compared to PLV. Thus, our simulations proved that the proposed modifications to existing metrics and new proposed measures were less affected by volume conduction compared to the original ones, as expected from theory.

Only a few previous studies tried to analyze the effects of volume conduction in various connectivity metrics simulating the volume conduction problem by means of different methods [10, 19, 16, 46]. Firstly, Stam *et al.* [10] used a 'simple' approximation based on linear mixing of Kuramoto oscillators. Then, they evaluated the ability of phase coherence (PC), PLI, and $iCOH$ to remain invariant against the presence of common sources. Their simulations showed that PLI responded to increases in the coupling strength of the oscillator and was less affected by volume conduction than PC and $iCOH$ [10]. Secondly, Ahmadi *et al.* [19] replicated this previous study employing the same model and calculating the same metrics as well others based on the visibility graph algorithms [47]. Their simulation results showed that PLI and visibility graph measures could predict the coupling degree correctly even in strongly overlapping environments [19]. Thirdly, Peraza *et al.* [46] used a simple head model based on four concentric-spheres to simulate the EEG activity at the scalp generated by surrogate sources located at the brain level. Then, they estimated PLI, $MSCOH$ and PC networks and calculated diverse parameters derived from graph theory. Agreeing with our results, they showed that $MSCOH$ and PC were highly affected by

volume conduction, while PLI was partially invariant to this effect [46]. Finally, Khadem *et al.* [16] tried to discriminate brain interactions and instantaneous linear mixing effects using two surrogate datasets. They ranked the estimated connectivity measures using a proposed sensitivity index, which quantifies the sensitivity of the metric to detect dependencies caused by brain interactions in the presence of instantaneous linear mixing effects [16]. Based on this rank and in line with our results, $iCOH$ and PLI (also weighted PLI) showed higher sensitivity levels compared to mutual information and $MSCOH$.

Therefore, taking into account previous findings and our results, which showed that PLI was the metric least affected by volume conduction effects, we could say that PLI could increase the insight into the underlying neural alterations at the different stages of AD.

5.2. Abnormal coupling patterns in AD progression

After reducing the possible bias that volume conduction could introduce by using PLI as a coupling metric, the characterization of neural changes in the AD progression was assessed. Our PLI results revealed that dementia due to AD is characterized by connectivity increases in low frequency bands and decreases in high frequency bands. Specifically, our results showed that EEG activity in MCI patients is characterized by a coupling increase in the θ band (see figure 4), and a decrease in the α and β_1 bands (see Supplementary Material, figures C and D), with only the connectivity increases being statistically significant. As dementia progresses, this increase in the θ band becomes more pronounced as more connections showed statistical differences. Furthermore, the aforementioned decrease in α band gets statistically significant at the last stage of dementia (AD_{sev}).

Only few previous studies analyzed the EEG connectivity changes in MCI [12, 48]. Tóth *et al.* [12] reported PLI decreases in patients diagnosed with an amnestic subtype of MCI at δ (0.5-4 Hz) and α_1 (8-10 Hz) frequency bands. Following the same trend, Babiloni *et al.* [48] estimated the source distribution of the electrical activity from the surface EEG data, and then they measured the functional connectivity between all regions of interest (ROIs). They reported that patients suffering from MCI due to AD showed statistically significant lower lagged linear connectivity values in the α frequency band, for both interhemispheric and intrahemispheric analyses [48]. Other previous EEG studies have shown evidences of functional connectivity loss for AD patients at the lower α band (8-10 Hz) in the posterior region, taking into account HC and three AD groups (AD_{mil}, AD_{mil}, and AD_{sev}) [49]. In line with our results, Stam *et al.* [50] found similar trends in spontaneous MEG activity of AD patients compared to HC subjects. Their mean PLI values were significantly lower for the AD group in the 8–10 Hz and 13–30 Hz bands. Additionally, their results also showed a non-significant coupling increase in the 4-8 Hz band, which agrees with our results in the θ band. Caunet *et al.* [51] found that source connectivity patterns between ROIs of AD patients (including AD_{mil}, AD_{mod}, and AD_{sev}, as the AD group) were characterized by a reduction of connectivity (by means of lagged phase synchronization) in the 10-13 Hz band and an increase in the θ band, involving mainly temporal and frontal connections. However, to the best of our knowledge, there is no previous study that analyzed the EEG activity stratifying the AD continuum in four groups from its prodromal form (MCI) to its last stage (AD_{sev}).

The proposed LDA model has shown the ability to detect whether a subject suffers from AD or MCI in 175 out of the 202 non-healthy subjects (Sensitivity = 86.63%), with a positive post-test probability of 87.94%. In addition, the model also showed the ability to confirm AD in 124 out of the 151 subjects suffering from this pathology (Sensitivity = 82.12%), with a positive post-test probability of 81.58%. A previous study carried out a classification approach using the same database and a leave-one-out cross-validation procedure [52]. They proposed a quadratic discriminant analysis model based on Multiscale Sample Entropy and Refined Multiscale Spectral Entropy results. They obtained a Cohen's kappa value of 0.2541, while our model obtained a slightly higher Cohen's kappa value (0.2688). Thus, our classification results highlight the diagnostic usefulness of our proposal, which might be used as an AD screening strategy.

Clinically, the variation of connectivity metrics reflects the underlying changes in amplitude and phase coupling of different oscillating neuronal populations. A well-known feature during AD continuum is the decrease in connectivity at high frequency bands between both close and distant channels, suggesting functional disconnections among cortical regions [53]. Some studies suggested that these connectivity decreases could be produced by structural brain changes, such as decreased hippocampal volume, atrophy of the medial temporal lobe or neuronal loss [54, 55]. Also, the disconnection between different brain areas could be due to global and regional gray matter density loss in AD patients, indicating an ongoing atrophic process in the brain [54]. Nevertheless, if the loss of neural coupling during neurodegeneration would simply be caused by a loss of neurons, it would be difficult to explain

why all frequencies are not equally affected [56]. Finally, another previous explanation for the observed decreases in α and β frequency bands is the loss of acetylcholine (a major excitatory modulator of cortical synaptic function), which led to the well-known 'cholinergic hypothesis of AD' [57, 58]. In addition, an animal study showed that the loss of acetylcholine results in a decrease in high-frequency coupling and an increase in low-frequency coupling [59]. Thus, the loss of acetylcholine could support our PLI results, explaining both the connectivity decrease in high frequency bands and the increase in low frequency bands during AD continuum.

5.3. Limitations and future research lines

In spite of the promising performance of PLI as a connectivity metric to detect changes in synchronization under simulated volume conduction conditions and its usefulness to characterize the brain alterations during the different stages of AD continuum, the present study has some limitations.

Firstly, although we analyzed the effect of volume conduction with the combination of a realistic surface-based head model and a model of Kuramoto oscillators, another way to mitigate this effect is to first solve the EEG inverse problem and then estimate functional connectivity between the estimated source activity. Solving the inverse problem could reduce the bias introduced by volume conduction, thus making source-connectivity results a more reliable estimation of the underlying coupling. However, the EEG inverse problem is ill-posed because for admissible output voltages, the solution is non-unique and unstable (the solution is highly sensitive to small changes in the noisy data) [60]. In most cases, an ill-conditioned equation has to be solved and some methods add spatial weighting of the current estimations at the source positions. These issues influence the estimation of source activity, so their results must be carefully interpreted [60].

Secondly, we simulated an isotropic electric propagation from cerebral sources to electrodes for all tissues. Some of the cerebral tissues, such as the white matter and the skull, present anisotropic conduction features that could influence connectivity results. This is an important issue to take into account in future studies, as it could lead to the construction of a more realistic brain model.

Thirdly, eight functional connectivity metrics were applied in this study to characterize their ability to detect real changes in synchronization without being affected by volume conduction. Our results revealed that none of them is immune to the volume conduction, despite these effects were smaller for PLI. Effective coupling metrics (e.g., Granger Causality, Cross-Sample Entropy, Partial Directed Coherence) might also have a similar performances under volume conduction conditions and could provide valuable information about neuronal organization.

Fourthly, even if we had a large database to characterize the brain abnormalities during the AD continuum, it would be useful to conduct a longitudinal study of subjects at early AD stages, such as MCI, to gain a deeper understanding on the complex neural changes of those that progress to AD and those remain stable in the MCI stage. Moreover, it could be also interesting to perform differential predictive diagnoses comparing AD and other neurodegenerative disorders in order to draw further clinical conclusions in future works.

Finally, starting from the weighted networks obtained by means of PLI, a complex analysis based on graph theory metrics could be addressed to characterize functional networks at the different stages of dementia due to AD. Other approaches using sub-networks, such as minimum spanning trees [61], may also provide valuable insights on the structural and functional organization of neural networks during the AD progression.

6. Conclusions

Our research provides an original approach to the characterization of EEG volume conduction using a real-head model and its effects on eight connectivity measures. We have proven that none of these metrics are immune to volume conduction, but PLI is the least affected. PLI has also proven its usefulness to reflect the neural changes caused by the AD progression in its different stages, from MCI to AD_{sev}. Our results suggest that functional connectivity increases in θ frequency band with increasing disease severity, meanwhile connectivity decreases in α band with the disease progression. Furthermore, we can conclude that all these findings are mainly due to neuronal alterations in dementia because we have used PLI, a metric that is slightly affected by volume conduction effects.

Acknowledgments

This research was supported by 'European Commission' and 'European Regional Development Fund' (FEDER) under project 'Análisis y correlación entre el genoma completo y la actividad cerebral para la ayuda en el diagnóstico de la enfermedad de Alzheimer' ('Cooperation Programme Interreg V-A Spain-Portugal, POCTEP 2014-2020'), by 'Ministerio de Ciencia, Innovación y Universidades' and FEDER under projects PGC2018-098214-A-I00 and DPI2017-

84280-R, and by 'Fundação para a Ciência e a Tecnologia/Ministério da Ciência, Tecnologia e Inovação' and FEDER under projects POCI-01-0145-FEDER-007274 and UID/MAT/00144/2013. Saúl J. Ruiz-Gómez was in receipt of a predoctoral scholarship from the 'Junta de Castilla y León' and the 'European Social Fund'.

References

[1] Babiloni C, Lizio R, Marzano N, Capotosto P, Soricelli A, Triggiani A I, Cordone S, Gesualdo L and Del Percio C 2016 Brain neural synchronization and functional coupling in Alzheimer's disease as revealed by resting state EEG rhythms *International Journal of Psychophysiology* **103** 88–102

[2] D'Amelio M and Rossini P M 2012 Brain excitability and connectivity of neuronal assemblies in Alzheimer's disease: From animal models to human findings *Progress in Neurobiology* **99** 42–60

[3] Alzheimer's Association 2017 2017 Alzheimer's Disease Facts and Figures *Alzheimers Dementia* **13** 325–373

[4] Petersen R C 2016 Mild cognitive impairment *Continuum (Minneap Minn)* **22** 404–418

[5] Davatzikos C, Bhatt P, Shaw L M, Batmanghelich K N and Trojanowski J Q 2011 Prediction of MCI to AD conversion, via MRI, CSF biomarkers, and pattern classification *Neurobiology of Aging* **32** 2322.e19–2322.e27

[6] Ewers M, Sperling R A, Klunk W E, Weiner M W and Hampel H 2011 Neuroimaging markers for the prediction and early diagnosis of Alzheimer's disease dementia *Trends in Neurosciences* **34** 430–442

[7] Martínez G, Vernooij R W, Fuentes Padilla P, Zamora J, Flicker L and Bonfill Cosp X 2017 18F PET with flutemetamol for the early diagnosis of Alzheimer's disease dementia and other dementias in people with mild cognitive impairment (MCI) *The Cochrane Database of Systematic Reviews* **11** 1–50

[8] Li H J, Hou X H, Liu H H, Yue C L, He Y and Zuo X N 2015 Toward systems neuroscience in mild cognitive impairment and Alzheimer's disease: A meta-analysis of 75 fMRI studies *Human Brain Mapping* **36** 1217–1232

[9] Poza J, Gómez C, García M, Corralejo R, Fernández A and Hornero R 2014 Analysis of neural dynamics in mild cognitive impairment and Alzheimer's disease using wavelet turbulence *Journal of Neural Engineering* **11** 26010

[10] Stam C J, Nolte G and Daffertshofer A 2007 Phase lag index: Assessment of functional connectivity from multi channel EEG and MEG with diminished bias from common sources *Human Brain Mapping* **28** 1178–1193

[11] Moretti D V, Frisoni G B, Pievani M, Rosini S, Geroldi C, Binetti G and Rossini P M 2008 Cerebrovascular disease and hippocampal atrophy are differently linked to functional coupling of brain areas: An EEG coherence study in MCI subjects *Journal of Alzheimer's Disease* **14** 285–299

[12] Tóth B, File B, Boha R, Kardos Z, Hidasi Z, Gaál Z A, Csibri É, Salacz P, Stam C J and Molnár M 2014 EEG network connectivity changes in mild cognitive impairment - Preliminary results *International Journal of Psychophysiology* **92** 1–7

[13] Ruiz-Gómez S J, Gómez C, Poza J, Martínez-Zarzuela M, Tola-Arribas M A, Cano M and Hornero R 2018 Measuring Alterations of Spontaneous EEG Neural Coupling in Alzheimer's Disease and Mild Cognitive Impairment by Means of Cross-Entropy Metrics *Frontiers in Neuroinformatics* **12** 1–11

[14] Poza J, Gómez C, García M, Tola-Arribas M A, Carreres A, Cano M and Hornero R 2017 Spatio-Temporal Fluctuations of Neural Dynamics in Mild Cognitive Impairment and Alzheimer's Disease. *Current Alzheimer Research* **14** 924–936

[15] Schoffelen J M and Gross J 2009 Source connectivity analysis with MEG and EEG *Human Brain Mapping* **30** 1857–1865

[16] Khadem A and Hossein-Zadeh G A 2014 Quantification of the effects of volume conduction on the EEG/MEG connectivity estimates: An index of sensitivity to brain interactions *Physiological Measurement* **35** 2149–2164

[17] Ewald A, Marzetti L, Zappasodi F, Meinecke F C and Nolte G 2012 Estimating true brain connectivity from EEG/MEG data invariant to linear and static transformations in sensor space *NeuroImage* **60** 476–488

[18] Nunez P L and Srinivasan R 2009 *Electric Fields of the Brain: The neurophysics of EEG* 3rd ed (New York: Oxford University Press Inc.)

[19] Ahmadi N, Pei Y and Pechenizkiy M 2019 Effect of linear mixing in EEG on synchronization and complex network measures studied using the Kuramoto model *Physica A: Statistical Mechanics and its Applications* **520** 289–308

[20] Mosher J C, Leahy R M and Lewis P S 1999 EEG and MEG: Forward solutions for inverse methods *IEEE Transactions on Biomedical Engineering* **46** 245–259

[21] Nolte G and Dassios G 2005 Analytic expansion of the EEG lead field for realistic volume conductors *Physics in Medicine and Biology* **50** 3807–3823

[22] Vorwerk J, Cho J H, Rampp S, Hamer H, Knösche T R and Wolters C H 2014 A guideline for head volume conductor modeling in EEG and MEG *NeuroImage* **100** 590–607

[23] Cho J H, Vorwerk J, Wolters C H and Knösche T R 2015 Influence of the head model on EEG and MEG source connectivity analyses *NeuroImage* **110** 60–77

[24] Kuramoto Y 1975 Self-entrainment of a population of coupled non-linear oscillators *International Symposium on Mathematical Problems in Theoretical Physics* vol 39 (Berlin, Heidelberg) pp 420–422

[25] Stam C J and van Straaten E C 2012 The organization of physiological brain networks *Clinical Neurophysiology* **123** 1067–1087

[26] McKhann G M, Knopman D S, Chertkow H, Hyman B T, Jack C R, Kawas C H, Klunk W E, Koroshetz W J, Manly J J, Mayeux R, Mohs R C, Morris J C, Rossor M N, Scheltens P, Carrillo M C, Thies B, Weintraub S and Phelps C H 2011 The diagnosis of dementia due to Alzheimer's disease: Recommendations from the National Institute on Aging-Alzheimer's Association workgroups on diagnostic guidelines for Alzheimer's disease *Alzheimer's and Dementia* **7** 263–269

[27] US National Library of Medicine The Visible Human Project URL `https://www.nlm.nih.gov/research/visible/visible_human.html`

[28] Makarov S N, Noetscher G M and Nazarian A 2016 *Low-Frequency Electromagnetic Modeling for Electrical and Biological Systems Using MATLAB* (Hoboken, New Jersey: John Wiley & Sons)

[29] Elloian J M, Noetscher G M, Makarov S N and Pascual-Leone A 2014 Continuous wave simulations on the propagation of electromagnetic fields through the human head *IEEE Transactions on Biomedical Engineering* **61** 1676–1683

[30] Noetscher G M, Yanamadala J, Makarov S N and Pascual-Leone A 2014 Comparison of cephalic and extracephalic montages for transcranial direct current stimulation-a numerical study *IEEE Transactions on Biomedical Engineering* **61** 2488–2498

[31] Yushkevich P A, Piven J, Hazlett H C, Smith R G, Ho S, Gee J C and Gerig G 2006 User-guided 3D active contour

segmentation of anatomical structures: Significantly improved efficiency and reliability *NeuroImage* **31** 1116–1128

[32] Strogatz S H 2000 From Kuramoto to Crawford: Exploring the onset of synchronization in populations of coupled oscillators *Physica D: Nonlinear Phenomena* **143** 1–20

[33] Ruiz-Gómez S J, Gómez C, Poza J, Maturana-Candelas A, Tola-Arribas M A, Cano M and Hornero R 2019 Analysis of Volume Conduction Effects on Different Functional Connectivity Metrics: Application to Alzheimer's Disease EEG Signals *Proceedings of the Annual International Conference of the IEEE Engineering in Medicine and Biology Society, EMBS* **Accepted for publication**

[34] Kiss I Z, Zhai Y and Hudson J L 2002 Emerging coherence in a population of chemical oscillators *Science* **296** 1676–1678

[35] Roach B J and Mathalon D H 2008 Event-related EEG time-frequency analysis: An overview of measures and an analysis of early gamma band phase locking in schizophrenia *Schizophrenia Bulletin* **34** 907–926

[36] Nolte G, Bai O, Wheaton L, Mari Z, Vorbach S and Hallett M 2004 Identifying true brain interaction from EEG data using the imaginary part of coherency *Clinical Neurophysiology* **115** 2292–2307

[37] Pascual-Marqui R D, Lehmann D, Koukkou M, Kochi K, Anderer P, Saletu B, Tanaka H, Hirata K, John E R, Prichep L, Biscay-Lirio R and Kinoshita T 2011 Assessing interactions in the brain with exact low-resolution electromagnetic tomography *Philosophical Transactions of the Royal Society A: Mathematical, Physical and Engineering Sciences* **2** 3768—3784

[38] O'Neill G C, Tewarie P, Vidaurre D, Liuzzi L, Woolrich M W and Brookes M J 2018 Dynamics of large-scale electrophysiological networks: A technical review *NeuroImage* **180** 559–576

[39] Brookes M J, O'Neill G C, Hall E L, Woolrich M W, Baker A, Palazzo Corner S, Robson S E, Morris P G and Barnes G R 2014 Measuring temporal, spectral and spatial changes in electrophysiological brain network connectivity *NeuroImage* **91** 282–299

[40] Stam C J and Van Dijk B W 2002 Synchronization likelihood: An unbiased measure of generalized synchronization in multivariate data sets *Physica D: Nonlinear Phenomena* **163** 236–251

[41] Lachaux J P, Rodriguez E, Martinerie J and Varela F J 1999 Measuring phase synchrony in brain signals *Human Brain Mapping* **8** 194–208

[42] Mormann F, Lehnertz K, David P and E Elger C 2000 Mean phase coherence as a measure for phase synchronization and its application to the EEG of epilepsy patients *Physica D: Nonlinear Phenomena* **144** 358–369

[43] Bruña R, Maestú F and Pereda E 2018 Phase locking value revisited: Teaching new tricks to an old dog *Journal of Neural Engineering* **15** 056011

[44] Benjamini Y and Hochberg Y 1995 Controlling the false discovery rate: a practical and powerful approach to multiple testing *Journal of the Royal Statistical Society B* **57** 289–300

[45] Bishop C M 2006 *Pattern Recognition and Machine Learning* (New York: Springer Science & Business Media) (*Preprint* 0-387-31073-8)

[46] Peraza L R, Asghar A U, Green G and Halliday D M 2012 Volume conduction effects in brain network inference from electroencephalographic recordings using phase lag index *Journal of Neuroscience Methods* **207** 189–199

[47] Lacasa L and Toral R 2010 Description of stochastic and chaotic series using visibility graphs *Physical Review E - Statistical, Nonlinear, and Soft Matter Physics* **82** 036120

[48] Babiloni C, Del Percio C, Pascarelli M T, Lizio R, Noce G, Lopez S, Rizzo M, Ferri R, Soricelli A, Nobili F, Arnaldi D, Famà F, Orzi F, Buttinelli C, Giubilei F, Salvetti M, Cipollini V, Franciotti R, Onofrj M, Stirpe P, Fuhr P, Gschwandtner U, Ransmayr G, Aarsland D, Parnetti L, Farotti L, Marizzoni M, D'Antonio F, De Lena C, Güntekin B, Hanoğlu L, Yener G, Emek-Savaş D D, Triggiani A I, Taylor J P, McKeith I, Stocchi F, Vacca L, Hampel H, Frisoni G B, De Pandis M F and Bonanni L 2019 Abnormalities of functional cortical source connectivity of resting-state electroencephalographic alpha rhythms are similar in patients with mild cognitive impairment due to Alzheimer's and Lewy body diseases *Neurobiology of Aging* **77** 112–127

[49] Engels M M, Stam C J, van der Flier W M, Scheltens P, de Waal H and van Straaten E C 2015 Declining functional connectivity and changing hub locations in Alzheimer's disease: An EEG study *BMC Neurology* **15**(145) 1–8

[50] Stam C J, De Haan W, Daffertshofer A, Jones B F, Manshanden I, Van Cappellen Van Walsum A M, Montez T, Verbunt J P, De Munck J C, Van Dijk B W, Berendse H W and Scheltens P 2009 Graph theoretical analysis of magnetoencephalographic functional connectivity in Alzheimer's disease *Brain* **132** 213–224

[51] Canuet L, Tellado I, Couceiro V, Fraile C, Fernandez-Novoa L, R I and Takeda M 2012 Resting-State Network Disruption and APOE Genotype in Alzheimer's Disease: A lagged Functional Connectivity Study *PLoS ONE* **7** 1–12

[52] Maturana-Candelas A, Gómez C, Poza J, Pinto N and Hornero R 2019 EEG characterization of the Alzheimer's disease continuum by means of multiscale entropies *Entropy* **21** 1–15

[53] Jeong J 2004 EEG dynamics in patients with Alzheimer's disease *Clinical Neurophysiology* **115** 1490–1505

[54] Karas G B, Scheltens P, Rombouts S A R B, Visser P J, Van Schijndel R A, Fox N C and Barkhof F 2004 Global and local gray matter loss in mild cognitive impairment and Alzheimer's disease *NeuroImage* **23** 708–716

[55] Cho H, Dong W Y, Young M S, Beum S K, Yeong I K, Young B C, Kwang S L, Yong S S, Yoon B, Kim W and Kook J A 2008 Abnormal integrity of corticocortical tracts in mild cognitive impairment: A diffusion tensor imaging study *Journal of Korean Medical Science* **23** 477–483

[56] Stam C J, Van Der Made Y, Pijnenburg Y A L and Scheltens P 2003 EEG synchronization in mild cognitive impairment and Alzheimer's disease *Acta Neurologica Scandinavica* **108** 90–96

[57] Bartus R, Dean R, Beer B and Lippa A 1982 The cholinergic hypothesis of geriatric memory dysfunction *Science* **217** 408–414

[58] Francis P T, Palmer A M, Snape M and Wilcock G K 1999 The cholinergic hypothesis of Alzheimer's disease: A review of progress *Journal of Neurology Neurosurgery and Psychiatry* **66** 137–147

[59] Villa A E, Tetko I V, Dutoit P and Vantini G 2000 Non-linear cortico-cortical interactions modulated by cholinergic afferences from the rat basal forebrain *BioSystems* **58** 219–228

[60] Grech R, Cassar T, Muscat J, Camilleri K P, Fabri S G, Zervakis M, Xanthopoulos P, Sakkalis V and Vanrumste B 2008 Review on solving the inverse problem in EEG source analysis *Journal of NeuroEngineering and Rehabilitation* **5** 1–33

[61] Tewarie P, van Dellen E, Hillebrand A and Stam C J 2015 The minimum spanning tree: An unbiased method for brain network analysis *NeuroImage* **104** 177–188